Higgs dynamics in the early universe

Vis, J.M. van de

Part II

Electroweak Baryogenesis

Chapter 5

Introduction to Electroweak Baryogenesis

The second part of this thesis focuses on a longstanding problem in particle physics and cosmology. Measurements show that there is an excess of matter over antimatter in our universe. The baryon asymmetry of the universe (BAU) is quantified by the ratio of of the baryon number density n_B (1/3 the number of quarks minus 1/3 the number of antiquarks) over the entropy density s. This quantity has been determined by two independent methods [11, 219]

$$Y_B = \frac{n_B}{s} = \begin{cases} 8.2\text{-}9.4 \times 10^{-11} & \text{Big Bang Nucleosynthesis}\,, \\ 8.65 \pm 0.09 \times 10^{-11} & \text{Planck}\,, \end{cases} \tag{5.1}$$

which are in good agreement.

If we assume that the universe started in a matter-antimatter symmetric state, the Standard Model can not explain how the observed baryon asymmetry was formed. Assuming that the universe started out with an overdensity of baryons does not solve the problem either: inflation would have washed out any initial density. Explaining the prevalence of baryons over antibaryons in our present universe thus requires a new mechanism to generate this asymmetry. This process is referred to as 'baryogenesis'. In the next section we will introduce the necessary conditions for baryogenesis and give examples of models that satisfy these conditions. We will then focus on a specific framework, electroweak baryogenesis, and explain how to fulfil the necessary condition of a first-order electroweak phase transition in section 5.2. In section 5.3 and 5.4 we derive the transport equations for the particles in the plasma. In section 5.5 we show how we compute the resulting baryon asymmetry. In this part of the thesis we use a metric with signature $(+,-,-,-)$.

5.1 Conditions for baryogenesis

5.1.1 Sakharov conditions

In 1967 Andrei Sakharov wrote down three conditions for successful baryogenesis [220]:

- **B violation**

  This condition is rather obvious: to go from a universe with no net baryon density to a universe with nonzero baryon number density, there should be some process in which baryon number is created. The standard model fulfils this condition through the non-perturbative electroweak sphaleron process [221, 222]. The electroweak sphaleron transition violates $B + L$ (baryon + lepton number). At low energies sphaleron transitions are exponentially suppressed but they are active at temperatures above the electroweak scale [223]. Extensive treatments of electroweak sphalerons in the context of baryogenesis can for example be found in Refs. [224–227].

- **C- and CP-violation**

  Violation of baryon number alone is not a sufficient condition. If C (charge) and CP (charge-parity) would be conserved, each baryon-number generating process would have a C- or CP-conjugate process that generated negative baryon number at the same rate. C- and CP-violation is thus a second condition for successful baryogenesis. The electroweak sector of the standard model violates C and the CKM-matrix accommodates CP-violation as well. The amount of CP-violation is however not sufficient to produce the observed baryon asymmetry [228–230].

- **Out-of-equilibrium dynamics**

  If the above two conditions were satisfied, but the relevant processes were in thermal equilibrium, baryogenesis would not occur. Deviation from thermal equilibrium is needed to ensure that baryon-number-generating processes do not have the same rate as their opposite processes, which destroy baryon number. An example of an out-of-equilibrium process is a first-order phase transition. For the measured value of the Higgs boson mass the electroweak phase transition is not first order [231–236]. The QCD phase transition is not first order either, so the condition of out-of-equilibrium dynamics is not satisfied in the standard model.

5.1.2 Models for baryogenesis

Understanding why baryons are more abundant than antibaryons thus requires BSM physics. There is a large range of BSM models that could explain the observed baryon asymmetry. In section 2.1.4 we already introduced two models in which the baryon asymmetry is generated during reheating (GUT-scale baryogenesis and Cold Electroweak Baryogenesis). Another important class of models are leptogenesis models. In this framework the SM is extended by heavy right-handed Majorana neutrinos. The out-of-equilibrium decay of these heavy particles generates a lepton asymmetry, which is (partly) converted into a baryon asymmetry by the electroweak sphalerons [237]. Leptogenesis is an attractive framework, since the heavy Majorana neutrinos could also explain the small left-handed neutrino masses through the see-saw mechanism [238–240].

The disadvantage of most leptogenesis and GUT baryogenesis models is that the BSM physics lives at a very high energy scale, decoupled from the electroweak scale. Such scenarios will be difficult to probe in current and upcoming experiments (although measurements of neutrinoless double beta decay would be a hint of leptogenesis). In this part of the thesis we will focus on the electroweak baryogenesis (EWBG) scenario [226, 227, 241], where the baryon asymmetry is generated during the electroweak phase transition. In this case, the scale of BSM physics cannot be much higher than the electroweak scale which makes the scenario more testable. In particular, searches for new scalars, precision measurements of Higgs couplings, and electric dipole moment (EDM) experiments all probe different aspects of EWBG scenarios.

5.1.3 Electroweak baryogenesis in a nutshell

The mechanism of EWBG is as follows. The Sakharov condition of out-of-equilibrium dynamics is satisfied if the electroweak phase transition is first order. The phase transition proceeds via the formation of bubbles of broken Higgs vacuum, which subsequently expand to eventually fill up all of space. The quarks and leptons in the plasma collide with the walls of the expanding bubbles. If these interactions violate CP, the transmission and reflection coefficients are different for particles and antiparticles. The net result is that an overdensity of left-handed particles over antiparticles builds up in front of the bubble wall. The $(B + L)$-violating electroweak sphaleron transitions only act on electroweak doublets, and transform this 'chiral asymmetry' into a net baryon number in front of the bubble. The produced baryons are then swept up by the expanding bubble. Inside the bubble the baryon number is preserved as the electroweak sphaleron processes are strongly suppressed in the broken vacuum. For reviews of EWBG, see for example Refs. [224–227].

5.2 The electroweak phase transition

For the measured value of the Higgs mass, the EWPT in the SM is a cross-over such that the Sakharov condition demanding an out-of-equilibrium process is not satisfied [231–236]. The SM Higgs potential needs to be supplemented by BSM physics that changes the phase transition to a first-order phase transition. We will use an effective dimension-six operator to parameterize the new physics:

$$\mathcal{L} \supset -\kappa(\Phi^\dagger\Phi)^3\,, \tag{5.2}$$

from the SM-EFT Lagrangian, where $\kappa = 1/\Lambda^2$ with Λ the scale of new physics. We define the components of the Higgs field as

$$\Phi = \frac{1}{\sqrt{2}}\begin{pmatrix} \theta^1 + i\theta^2 \\ \varphi + h + i\theta \end{pmatrix}, \tag{5.3}$$

with θ^i the Goldstone bosons, h the Higgs field, and φ the background field, the tree-level classical potential in terms of φ is given by

$$V_0 = \frac{\mu^2}{2}\varphi^2 + \frac{\lambda}{4}\varphi^4 + \frac{\kappa}{8}\varphi^6\,. \tag{5.4}$$

5.2.1 The finite-temperature Higgs potential

In order to describe the phase transition we need to include loop corrections to the potential. The one-loop effective potential can be split into the zero-temperature Coleman-Weinberg potential and the finite-temperature contribution. The former can be resummed to get the renormalization group improved effective potential where the couplings are running with scale. For the analysis of EWBG we use the coupling values at the renormalization scale $M = m_Z$, and for simplicity neglect all running effects and threshold corrections. The calculation of the finite temperature contribution V_T is reviewed in Appendix A.1 of Ref. [3]. We can write the one-loop effective potential as $V_{\text{eff}} = V_{\text{RG}} + V_T$, with V_{RG} the RG-improved potential, and

$$V_{\text{eff}} = \frac{\mu^2}{2}\varphi^2 + \frac{\lambda}{4}\varphi^4 + \frac{\kappa}{8}\varphi^6 + \sum_X n_X \frac{T^4}{2\pi^2} J_B(m_X^2/T^2) - \sum_f n_f \frac{T^4}{2\pi^2} J_F(m_f^2/T^2)\,, \tag{5.5}$$

where we take μ, λ and κ at the renormalization scale. The sums are over all bosons X and fermions f that couple to the Higgs. We only include the fermion contribution from the top quark. n_X and

n_f denote the numbers of degrees of freedom and are given by $n_{\{h,\theta,W,Z,t\}} = \{1, 3, 6, 3, 4N_c\}$, with N_c the number of colors. The functions $J_{B,F}$ are given by

$$J_{B,F}\left(m^2/T^2\right) = \int_0^\infty dk k^2 \log\left[1 \mp e^{\left[-\sqrt{k^2+m^2/T^2}\right]}\right], \tag{5.6}$$

with the upper (lower) sign for bosons (fermions). In the high-temperature expansion (see eq. (A.11) of Ref. [3] for the expansion of J_B and J_F) the potential becomes

$$V_{\text{eff}} = \left(\frac{\mu^2}{2} + \frac{a_T}{2}T^2\right)\varphi^2 + \left(\frac{\lambda}{4} + \frac{b_T}{4}T^2\right)\varphi^4 + \frac{\kappa}{8}\varphi^6 + \mathcal{O}(T\varphi^3)\,, \tag{5.7}$$

where

$$a_T = \frac{1}{16}\left(\frac{4m_h^2}{v_0^2} + 3g^2 + g'^2 + 4y_t^2 - 12v_0^2\kappa\right), \qquad b_T = \kappa\,, \tag{5.8}$$

with m_h and v_0 the zero-temperature Higgs mass and Higgs vev, respectively. For simplicity, we will use this high-temperature expansion to determine the allowed values of κ, and to find the Higgs profile across the bubble wall that is used for the calculation of the baryon asymmetry. In addition, we neglect higher-loop corrections due to ring diagrams (usually called daisy resummation), and as mentioned above evaluate all running couplings at the scale of the Z-boson mass, and neglect further running and threshold effects. The results are not significantly different from those obtained with the full potential [242], in which all these effects are included. The simplified potential is sufficient for the goals of the upcoming two chapters: testing the SM-EFT framework and comparing the contributions of different fermions to the baryon asymmetry.

5.2.2 Nucleating bubbles

At very high temperatures the effective Higgs potential only has a minimum at $\varphi = 0$, while for lower temperatures a second minimum appears. In a potential that allows for a first-order EWPT the two minima are degenerate at some critical temperature T_c. The value of the field φ in the second minimum is denoted by v_c. We find degenerate minima for κ in the range $1.6 < (\kappa \times \text{TeV}^2) < 4.3$, in agreement with Refs. [242, 243].

The EWPT proceeds by the formation of bubbles of broken vacuum. If larger than some critical size, these bubbles expand and eventually fill up the entire universe. While bubbles can already form at the critical temperature, their rate may be too small for the phase transition to complete. The temperature at which tunnelling to the true vacuum proceeds is called the nucleation temperature T_N. To obtain this temperature we follow the discussion in Refs. [242, 244].

The tunnelling rate is $\Gamma \propto e^{-S_E}$, with S_E the Euclidean action for the so-called bounce solution φ_b [245]. At temperatures T greater than the inverse bubble radius R^{-1}, the bounce solution is $O(3)$-symmetric [246] and obeys the equation

$$\frac{d^2\varphi_b}{dr^2} + \frac{2}{r}\frac{d\varphi_b}{dr} - \frac{\partial V_{\text{eff}}(\varphi_b, T)}{\partial \varphi_b} = 0\,, \tag{5.9}$$

with boundary conditions

$$\varphi_b(r \to \infty) = 0 \quad \text{and} \quad \frac{d\varphi_b(r=0)}{dr} = 0\,. \tag{5.10}$$

$\varphi_b(r)$ gives the field profile of a static bubble, with r the distance from the center of the bubble. The corresponding Euclidean action factorizes into $S_E = S_3/T$, with

$$S_3 = 4\pi \int dr r^2 \left[\frac{1}{2}\left(\frac{d\varphi_b}{dr}\right)^2 + V_{\text{eff}}(\varphi_b, T)\right]\,. \tag{5.11}$$

Nucleation happens when the probability of creating a single bubble within one horizon is of order one [247], which leads to the condition

$$\frac{S_3}{T_N} \simeq 140\,. \tag{5.12}$$

The field value at the center of the bubbles at T_N is denoted by v_N. We point out that v_N is slightly smaller than the field value at the minimum of the potential. The difference between v_N and the field value at the minimum is larger when there is a large difference between the potential in the true and the false vacuum.

We use the Mathematica Package 'AnyBubble' [248] to solve the bounce equation (5.9) and compute S_3 for $\kappa = 2$, 2.5, and $3\,\text{TeV}^{-2}$. Figure 5.1 shows S_3/T as a function of temperature. For $\kappa \gtrsim 3\,\text{TeV}^{-2}$, the minimum of the potential at $\varphi = 0$ persists until $T = 0$, which is reflected in the figure by the lower bound on S_3/T. The nucleation rate is never large enough, and φ gets trapped in the symmetric vacuum. For $\kappa \lesssim 1.8\,\text{TeV}^{-2}$ the minimum at $\varphi = 0$ changes into a maximum before bubbles have had time to nucleate, and the EWPT is not first order.

In order to preserve the baryon number that was formed in the broken phase, the sphaleron transitions should be suppressed inside the bubble. The rate of sphaleron transitions inside the bubble is proportional to $\exp\left[-E_{\text{sph}}(T_N)/T_N\right]$, with the sphaleron energy $E_{\text{sph}}(T_N)$ being proportional to v_N. We therefore demand the additional condition for baryogenesis $v_N/T_N \gtrsim 1$ and refer to Refs. [249, 250] for a more detailed discussion. We find that this is automatically assured for all

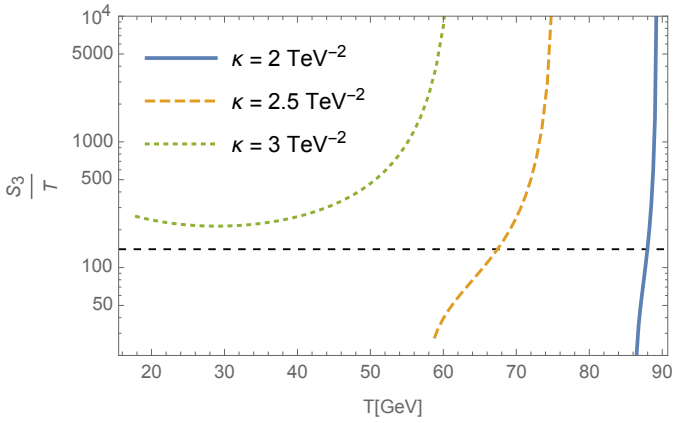

FIGURE 5.1: S_3/T as a function of temperature for three values of κ. The horizontal line indicates $S_3/T = 140$, the approximate value for which bubbles nucleate. The graph shows that nucleation is impossible for $\kappa \gtrsim 3\,\text{TeV}^{-2}$.

values of κ for which a first-order phase transition is possible in the first place. The strength of the phase transition and the value of v_N/T_N increases with κ.

To summarize, only for a narrow range of values for κ do we satisfy all criteria for successful baryogenesis:

$$1.8 \lesssim (\kappa \times \text{TeV}^2) \lesssim 3\,. \tag{5.13}$$

If we write $\kappa = \Lambda^{-2}$ this corresponds to the scale $0.58\,\text{TeV} < \Lambda < 0.75\,\text{TeV}$.

Finally, we briefly discuss the bubble profile which is needed to calculate the baryon asymmetry. The bounce solution $\varphi_b(r)$ is the initial time ($t = 0$) bubble profile. In the rest frame of the bubble, the solution at later times is $\varphi_b(\tilde{z})$ with $\tilde{z} = |r - v_w t|$, with v_w the radial velocity of the bubble wall. We can define a new variable

$$z = r_c - \tilde{z} = r_c - |r - v_w t|\,, \tag{5.14}$$

with r_c the location of the bubble wall defined via $\varphi_b(r_c) = \varphi_b(0)/2$. In terms of this new coordinate the bubble wall is located at $z = 0$, with the broken phase at $z > 0$ and the symmetric phase at $z < 0$, which matches a convention often used in the literature. We can now write the bubble profile solution $\varphi_b(\tilde{z}(z))$ as a function of z. To calculate the baryon asymmetry the wall curvature is usually neglected, and the bubble is approximated by a plane located at $z = 0$; in this approximation r can be replaced by the coordinate perpendicular to the wall, and z is extended to $\pm\infty$.

In the literature the bubble profile is often parametrized by a kink solution [251]

$$\varphi_b^{\text{kink}} = \frac{v_N}{2}\left(1 + \tanh\frac{z}{L_w}\right)\,, \tag{5.15}$$

where L_w is a measure of the width of the bubble wall. The numerical solution can be fit to this parametrization to extract L_w. We will use the kink solution in chapter 7.

5.3 CP-violating source terms

The number densities of the plasma particles in the presence of an expanding bubble are governed by transport equations. To obtain a baryon asymmetry, these equations need to include a CP-violating (CPV) source term that drives the chiral asymmetry. We will use dimension-six CPV operators from the Standard Model Effective Field Theory (SM-EFT) that we will specify in chapters 6 and 7. For definiteness we will now consider a CPV top-Higgs interaction:

$$\mathcal{L}_6^{\rm CPV} = -\frac{i}{\Lambda_{\rm CP}^2}\bar{Q}_L y_t \tilde{\Phi} t_R (\Phi^\dagger \Phi) + \text{h.c.}\,, \tag{5.16}$$

where Q_L denotes the left-handed doublet of the third generation and t_R the right-handed top. Φ denotes the Higgs doublet and $\tilde{\Phi}^a = \epsilon^{ab}\Phi^{b*}$. $\Lambda_{\rm CP}$ is the scale of new physics. We will just sketch the derivation of the transport equations, focusing on how this source term depends on the bubble wall profile. More details can be found in Ref. [252], the methods of which we follow.

The quantum transport equations are derived in the finite temperature Closed-Time-Path formalism [138, 139, 253–256]. Starting from the Schwinger-Dyson equation a transport equation for the number current of top quarks can be derived

$$\begin{aligned}\partial_\mu j_i^\mu(x) = -\int d^3z \int_{-\infty}^{x_0} dz_0 \ \mathrm{Tr}\Big[&\Sigma_i^>(x,z)S_i^<(z,x) - S_i^>(x,z)\Sigma_i^<(z,x) \\ &+ S_i^<(x,z)\Sigma_i^>(z,x) - \Sigma_i^<(x,z)S_i^>(z,)\Big]\,,\end{aligned} \tag{5.17}$$

with $i = L, R$ for the left- and right-handed top quark respectively. Here S^λ are the fermionic Wightman functions (see Ref. [252] for the explicit definitions), and Σ^λ the corresponding self-energies defined below in eq. (5.20).

In the bubble background the fermion mass is space-time dependent as it depends on the Higgs background $\varphi_b(z)$. To deal with this complication, the self-energies are calculated in the 'vev-insertion approximation' (VIA) [257–260], which amounts to treating the field-dependent part of the mass as a perturbation. The zero-temperature top mass m_t can be split into a real and imaginary part (indicated by superscripts), and likewise for the thermal corrections δm_t. The quadratic Lagrangian for the top quarks is split into a free part, independent of the bubble profile, and a field-dependent

interaction part, according to

$$\mathcal{L}^{\text{free}} \supset \sum_{i=L,R} \bar{t}_i \left(i\not{\partial} - \delta m_i^{\text{Re}}(T) \right) t_i \,, \tag{5.18}$$

$$\mathcal{L}^{\text{int}} \supset -\left[m_t^{\text{Re}}(\varphi_b) + i \left(m_t^{\text{Im}}(\varphi_b) + \delta m_t^{\text{Im}}(\varphi_b, T) \right) \right] \bar{t}_L t_R + \text{h.c.} \equiv -\frac{\mathscr{g}_t(T, \varphi_b)}{\sqrt{2}} \bar{t}_L t_R + \text{h.c.} \,. \tag{5.19}$$

The $\mathscr{g}_t$-functions defined above, which parameterize the interaction strength, depend on the specific CPV-interaction and will be given in chapters 6 and 7. The $\delta m_i^{\text{Re}}(T)$ are the usual SM thermal masses [261]. They can be viewed as one-loop thermal corrections to the massless propagator. Since these corrections do not depend on the space-time dependent Higgs profile, they can be resummed and included in the full propagator $S_i^{\lambda}(\delta m_i^{\text{Re}})$, which is constructed from the free Lagrangian. The $\delta m_i^{\text{Im}}(\varphi_b, T)$ are the one-loop thermal corrections to the CPV m_i^{Im}-vertex. All the terms in $\mathscr{g}_t$ are field dependent, and therefore treated as a perturbation. The imaginary part of the mass is space-time dependent in the bubble background, and cannot be rotated away by a chiral transformation if it is non-linear in the field. Its presence leads to different dispersion relations for left- and right-handed particles, and consequently different forces act on them as they scatter with the bubble wall. This is the physical underpinning of the appearance of a source term, denoted by $S^{\not{\text{CP}}}$, in the transport equations that drives the chiral asymmetry. Based on this discussion, we expect $S^{\not{\text{CP}}} \propto \text{Im}(\mathscr{g}_t' \mathscr{g}_t^*)$, where a prime denotes a derivative with respect to z, the distance from the center of the bubble wall. This specific combination of $\mathscr{g}_t$ and $\mathscr{g}_t'$ arises as the source should be proportional to $\mathscr{g}_t'$, depend on the phase of $\mathscr{g}_t$, and be quadratic in $\mathscr{g}_t$ as the diagram for $t_L \to t_L$ scattering requires at least two mass insertions. This dependence is confirmed by the explicit derivation, which we will now sketch.

We consider the transport equation for the right-handed top quark t_R. The self-energy Σ_R^{λ} obtains a contribution from the diagram with two mass insertions

$$\Sigma_R^{\lambda}(x, y) = -\frac{1}{2} \mathscr{g}_t(x) \mathscr{g}_t^*(y) P_R S_L^{\lambda}(x, y) P_L \,, \tag{5.20}$$

with $P_{L,R}$ the left- and right-handed projection operators. Using eq. (5.20) in the transport equation (5.32), we can separate the right-hand side into a real and imaginary part, corresponding to the

CP-conserving relaxation term and the CPV source

$$\begin{aligned}\partial_\mu j^\mu_R(x) &= \frac{1}{4}\int d^3z \int_{-\infty}^{x_0} dz_0 \;\left[\not{g}_t(x)\not{g}_t(z)^* + \not{g}_t(x)^*\not{g}_t(z)\right]\;\mathrm{Re}\,\mathrm{Tr}\left[S^>_{L,xz}S^<_{R,zx} - S^<_{L,xz}S^>_{R,zx}\right]_{\mathrm{Tr}(m)=0}\\ &+ \frac{1}{4}\int d^3z \int_{-\infty}^{x_0} dz_0\, i\left[\not{g}_t(x)\not{g}_t(z)^* - \not{g}_t(x)^*\not{g}_t(z)\right]\;\mathrm{Im}\,\mathrm{Tr}\left[S^>_{L,xz}S^<_{R,zx} - S^<_{L,xz}S^>_{R,zx}\right]_{\mathrm{Tr}(m)=0}\\ &= S^{\mathrm{CP}}_R(x) + S^{\not{\mathrm{CP}}}_R(x)\,, \end{aligned} \tag{5.21}$$

where we used the short-hand$S^{\lessgtr}_{i,xz} = S^{\lessgtr}_i(x,z)$. The subscript $\mathrm{Tr}(m)=0$ indicates that the mass can be set to zero in the trace of the propagators[1]. The analogous equation can be written down for the left-handed fermion, with $S^{\mathrm{CP}}_L(x) = -S^{\mathrm{CP}}_R(x)$ and $S^{\not{\mathrm{CP}}}_L(x) = -S^{\not{\mathrm{CP}}}_R(x)$.

In the limit that the typical time scale for thermalization of the fermions is much faster than the time scale on which the Higgs profile changes, we can expand[2]

$$\begin{aligned}\lim_{z\to x}\left[\not{g}_t(x)\not{g}_t(z)^* + \not{g}_t(x)^*\not{g}_t(z)\right] &\approx 2|\not{g}_t(x)|^2\,,\\ \lim_{z\to x}\left[\not{g}_t(x)\not{g}_t(z)^* - \not{g}_t(x)^*\not{g}_t(z)\right] &\approx 2iv_w\mathrm{Im}[\not{g}_t'(x)\not{g}_t(x)^*](x^0-z^0)\,,\end{aligned} \tag{5.23}$$

and the $\not{g}_t$-dependent parts can be taken outside the z-integral in eq. (5.21). This gives the result we are after, as it factors out the explicit dependence on the bubble-wall profile. We find that $S^{\mathrm{CP}}_R \propto |\not{g}_t|^2$, explicitly

$$S^{\mathrm{CP}}_R = \Gamma^+(\mu_L+\mu_R) + \Gamma^-(\mu_L-\mu_R)\,, \tag{5.24}$$

with $\mu_{L,R}$ the chemical potentials of left- and right-handed top quarks respectively. The rates $\Gamma^\pm$ are given by

$$\begin{aligned}\Gamma^\pm = \frac{6}{T^2}\times\frac{N_c}{4\pi^2T}|\not{g}_t|^2\int\frac{k^2\mathrm{d}k}{\omega_L\omega_R}\mathrm{Im}\Bigg[&-\frac{(h(\mathcal{E}_L)\mp h(\mathcal{E}^*_R))}{\mathcal{E}^*_R-\mathcal{E}_L}\left(\mathcal{E}_L\mathcal{E}^*_R - k^2\right)\\ &+\frac{(h(\mathcal{E}_L)\mp h(\mathcal{E}_R))}{\mathcal{E}_L+\mathcal{E}_R}\left(\mathcal{E}_L\mathcal{E}_R + k^2\right)\Bigg]\,,\end{aligned} \tag{5.25}$$

[1]Inserting eq. (5.20) into eq. (5.32) gives a trace of a product of propagators and projection operators, which in Fourier space is of the form $\mathrm{Tr}\left[P_L(\not{p}+m_i)P_R(\not{q}+m_j)\right] = \frac{1}{2}\mathrm{Tr}\left[\not{p}\not{q}\right]$. By defining

$$S^\lambda_i(x)\big|_{\mathrm{Tr}(m)=0} = \int\frac{\mathrm{d}^4k}{(2\pi)^4}\mathrm{e}^{ik.x}\hat{S}^\lambda_i(k)(\not{k}+m)\Big|_{\mathrm{Tr}(m)=0} = \int\frac{\mathrm{d}^4k}{(2\pi)^4}\mathrm{e}^{ik.x}\hat{S}^\lambda_i(k)\not{k}\,, \tag{5.22}$$

(5.21) can be neatly split into a CP-conserving and CPV part.

[2]Here we used that Taylor expanding $\lim_{z\to x}\left[\not{g}_t(x)\not{g}_t(z)^* - \not{g}_t(x)^*\not{g}_t(z)\right]$, the $\not{g}_t^*\partial_i\not{g}_t$ term vanishes when substituted in the integral in eq. (5.21) because of spatial isotropy, and thus only the term proportional to the time-derivative $\not{g}_t^*\partial_0\not{g}_t = v_w\not{g}_t^*\not{g}_t'$ contributes [252].

with T the temperature, $h(x) = e^{x/T}(e^{x/T}+1)^{-2}$ the derivative of the Fermi-Dirac distribution $n_f(x) = (e^{x/T}+1)^{-1}$ and

$$\omega_i = \sqrt{k^2 + (\delta m_i^{\rm Re})}\,, \qquad \mathcal{E}_i = \omega_i - i\Gamma_t\,, \tag{5.26}$$

with Γ_t the thermal width. We will set Γ^+ to zero, which is a good approximation, and switch to the notation $\Gamma_M \equiv \Gamma^-$. The expression for the CPV source term is

$$\begin{aligned} S_R^{\not{CP}} = \frac{v_w N_c}{2\pi^2}\mathrm{Im}[\not{g}_t'\not{g}_t^*]\int \frac{k^2\mathrm{d}k}{\omega_L\omega_R}\mathrm{Im}\Bigg[&\frac{(n_f(\mathcal{E}_L)-n_f(\mathcal{E}_R^*))}{(\mathcal{E}_L-\mathcal{E}_R^*)^2}\left(\mathcal{E}_L\mathcal{E}_R^*-k^2\right) \\ &+\frac{(n_f(\mathcal{E}_L)+n_f(\mathcal{E}_R)-1)}{(\mathcal{E}_L+\mathcal{E}_R)^2}\left(\mathcal{E}_L\mathcal{E}_R+k^2\right)\Bigg]. \end{aligned} \tag{5.27}$$

The '-1' term in the numerator on the second line gives a divergent contribution that survives in the zero-temperature limit where the distributions n_f are Boltzmann suppressed. This divergence is absorbed by the counterterms of the zero-temperature renormalized action, or equivalently, this term can be removed by normal ordering the operators [262].

In the computation of these terms we have neglected collective plasma excitations (hole modes) [263–265]. The expressions for the source terms and relaxation rates for any fermion f can be obtained by using $\not{g}_f$ and the quantities ω_i and $\mathcal{E}_i$ corresponding to the fermion f. In appendix A the thermal widths, thermal masses and couplings needed for the computation of the CPV source and relaxation rates are listed. For leptons we set $N_c = 1$.

An alternative approach for the computation of the source terms is the semi-classical method of Refs. [266–268], which uses the WKB expansion, and is also valid for large Yukawa couplings. The source term does not depend on the thermal corrections. The expression found in Ref. [268] (multiplied by $T^3/6$ to match our conventions) for a fermion f is

$$S_f^{\rm WKB} = \frac{c v_w N_c D_f}{24}(|\not{g}_f|^2\theta'_{\not{g}_f})'\,, \tag{5.28}$$

with $c = \mathcal{O}(1)$, D_f the diffusion constant, and $\theta_{\not{g}_f} = \arg(\not{g}_f)$. Since it is third order in the derivative expansion it is a factor $(L_w T_N)^{-2} \sim 10^{-2}$ suppressed with respect to the source in eq. (7.4), where we used the benchmark values listed in Appendix A. Including all numerical factors negates this suppression: for the benchmark values of chapters 6 and 7 we find that the semi-analytical and VIA source terms are of the same order of magnitude $S_f^{\rm WKB}/S_f = 0.2-5$, with the larger values obtained for leptons (which have larger diffusion constants). For definiteness, in the upcoming chapters we will use the source term in eq. (5.27) (and also the CP-conserving relaxation rate) derived in VIA for

all fermions. The qualitative results on the applicability of the SM-EFT and the role of leptons in EWBG will not depend on this, and the results can straightforwardly be adapted to different source terms.

Apart from the just derived CP-conserving rate Γ_M and CP-violating source term $S^{\not{C}\not{P}}$, the SM Yukawa interaction also enters the transport equations. The 3-point $\bar{t}_L t_R h$-interactions is kinematically forbidden (the same is the case for other fermions), so we include the 4-point $\bar{t}_L t_R h g$ interaction, which has an extra gluon line [269]:

$$\Gamma_Y = \Gamma_Y^{(4)} = \frac{\zeta_3}{6\pi^2} g_s^2 |\not{g}_t|^2 T \ln\left(\frac{8T^2}{m_q^2}\right) , \tag{5.29}$$

where we take for the typical mass scale $m_q = \delta m_t^{\mathrm{Re}}$, or the appropriate mass when we consider a different fermion. Like above, the expression for Γ_Y neglects collective plasma excitations.

Finally, another rate that goes into the transport equations is the strong sphaleron rate [270]

$$\Gamma_{ss} = 14\kappa' \alpha_s^4 T , \tag{5.30}$$

where we take $\kappa' = 1$. Strong sphaleron interactions only affect quarks.

5.4 Quantum Boltzmann transport equations

We are now ready to write down the quantum Boltzmann transport equations for a system with CP-violating sources for top and bottom quark as well as the tau lepton, generalizing the results of Refs. [252, 271]. From these equations we can compute the density of left-handed particles. This density sources the electroweak sphaleron transition that generates a net baryon number. We denote the net number density — meaning the number density of particles minus antiparticles — of third-generation quarks by $t = n_{t_R}$, $b = n_{b_R}$, $q = n_{t_L} + n_{b_L}$, the third-generation leptons by $\nu = n_{\nu_R}$, $\tau = n_{\tau_R}$, $l = n_{\nu_L} + n_{\tau_L}$, and similarly for the lighter generations; the Higgs number density is given by $h = n_{\Phi^0} + n_{\Phi^+}$.

Gauge interactions and Higgs self-interactions are fast compared to the relevant time scales and are therefore assumed to be in thermal equilibrium, implying that the chemical potentials of the up and down components of $SU(2)_L$ doublets are equal. The same holds for the components of the Higgs doublet. First- and second-generation Yukawa interactions are slow and are therefore neglected; we justify this approximation in chapter 7. Consequently, the light leptons effectively decouple. The

light quarks still participate in strong sphaleron interactions, which means their densities are related via

$$q_1 = q_2 = -2u = -2d = -2s = -2c\,, \tag{5.31}$$

and we only require one equation to describe them. We choose the u-quark. Here q_i denotes the first- and second-generation left-handed doublet, and u, d, s, c the right-handed quarks. If we neglect the bottom Yukawa interactions, we have the further simplification $u = b$.

Weak sphaleron processes are also slow and baryogenesis can be modeled as a two-step process, where in the first step a chiral asymmetry is generated, which in a second step is converted into a baryon asymmetry [257, 268]. We argue in section 7.3 that this two-step approach even works for a lepton source scenario, where the relevant tau-Yukawa interaction rate can be small compared to the weak sphaleron rate. The conversion of the chiral asymmetry into a baryon asymmetry is described in section 5.5.

With the above considerations the full set of transport equations becomes

$$\begin{aligned}
\partial_\mu q^\mu &= +\Gamma_M^{(t)}\mu_M^{(t)} + \Gamma_M^{(b)}\mu_M^{(b)} + \Gamma_Y^{(t)}\mu_Y^{(t)} + \Gamma_Y^{(b)}\mu_Y^{(b)} - 2\,\Gamma_{\rm ss}\,\mu_{\rm ss} - S_t - S_b\,,\\
\partial_\mu t^\mu &= -\Gamma_M^{(t)}\mu_M^{(t)} - \Gamma_Y^{(t)}\mu_Y^{(t)} + \Gamma_{\rm ss}\,\mu_{\rm ss} + S_t\,,\\
\partial_\mu b^\mu &= -\Gamma_M^{(b)}\mu_M^{(b)} - \Gamma_Y^{(b)}\mu_Y^{(b)} + \Gamma_{\rm ss}\,\mu_{\rm ss} + S_b\,,\\
\partial_\mu l^\mu &= +\Gamma_M^{(\tau)}\mu_M^{(\tau)} + \Gamma_Y^{(\tau)}\mu_Y^{(\tau)} - S_\tau\,,\\
\partial_\mu \nu^\mu &= 0,\\
\partial_\mu \tau^\mu &= -\Gamma_M^{(\tau)}\mu_M^{(\tau)} - \Gamma_Y^{(\tau)}\mu_Y^{(\tau)} + S_\tau\,,\\
\partial_\mu h^\mu &= +\Gamma_Y^{(t)}\mu_Y^{(t)} - \Gamma_Y^{(b)}\mu_Y^{(b)} + \Gamma_Y^{(c)}\mu_Y^{(c)} - \Gamma_Y^{(\tau)}\mu_Y^{(\tau)}\,,\\
\partial_\mu u^\mu &= +\Gamma_{\rm ss}\mu_{\rm ss}\,.
\end{aligned} \tag{5.32}$$

The S_f denote the flavor-diagonal CPV sources for third-generation fermions that we derived in section 5.3, with $f = t, b, \tau$. The relaxation rates $\Gamma_M^{(f)}$, Yukawa rates $\Gamma_Y^{(f)}$, and strong sphaleron rate $\Gamma_{\rm ss}$, redistribute and/or wash out the generated chiral asymmetry. The lepton sector mirrors the quark sector in the above equations, with the important difference that the leptons do not have strong sphaleron transitions, and the right-handed neutrino decouples.

The chemical potentials (strictly speaking, these are rescaled chemical potentials, as we have factored out a factor $6/T^2$) corresponding to the interaction rates $\Gamma_M^{(f)}$, $\Gamma_Y^{(f)}$ and $\Gamma_{\rm ss}$ are

$$\begin{aligned}
\mu_M^{(t)} &= \left(\frac{t}{k_t} - \frac{q}{k_q}\right), & \mu_Y^{(t)} &= \left(\frac{t}{k_t} - \frac{q}{k_q} - \frac{h}{k_h}\right), \\
\mu_M^{(b)} &= \left(\frac{b}{k_b} - \frac{q}{k_q}\right), & \mu_Y^{(b)} &= \left(\frac{b}{k_b} - \frac{q}{k_q} + \frac{h}{k_h}\right), \\
\mu_M^{(\tau)} &= \left(\frac{\tau}{k_\tau} - \frac{l}{k_l}\right), & \mu_Y^{(\tau)} &= \left(\frac{\tau}{k_\tau} - \frac{l}{k_l} + \frac{h}{k_h}\right), \\
\mu_{\rm ss} &= \sum_{i=1}^{3}\left(\frac{2q_i}{k_{q_i}} - \frac{u_i}{k_{u_i}} - \frac{d_i}{k_{d_i}}\right).
\end{aligned} \tag{5.33}$$

The $k_i(m_i/T)$-functions relating the chemical potentials to the number densities are defined via $n_i = T^2\mu_i k_i/6 + \mathcal{O}(\mu_i^3)$ and their expression is:

$$k_i(m/T) = k_i(0)\frac{c_{F,B}}{\pi^2}\int_{m/T}^{\infty} dx x \frac{e^x}{(e^x \pm 1)^2}\sqrt{x^2 - \frac{m^2}{T^2}}\,, \tag{5.34}$$

where $c_{F(B)} = 6\,(3)$ and the $+(-)$ sign in the denominator is for fermions (bosons), and

$$k_{Q_L}(0) = 6\,, \quad k_{q_R}(0) = 3\,, \quad k_{L_L}(0) = 2\,, \quad k_{l_R}(0) = 1\,, \quad k_\Phi(0) = 4\,, \tag{5.35}$$

where Q_L (L_L) denotes any left-handed quark (lepton) doublet, q_R (l_R) any right-handed quark (lepton) singlet and Φ the Higgs doublet.

It is easiest to work in the rest frame of the bubble, where the Higgs profile is only a function of $z = r_c - |r - v_w t|$ as in eq. (5.14), and we can express all space-time derivatives in terms of z-derivatives. In the diffusion approximation the current can be written as $j_i^\mu = (n_i, -D_i\vec{\nabla}n_i)$ with n_i the number densities and D_i the diffusion coefficients. In addition, we neglect the curvature of the bubble wall, and model the bubble wall as a plane located at $z = 0$ [272]. With these approximations

$$\partial_\mu n_f^\mu(x) \simeq v_w n_f' - D_f\vec{\nabla}^2 n_f \simeq v_w n_f' - D_f n_f''\,, \tag{5.36}$$

where the last expression is valid for the planar approximation, and where a prime denotes a derivative with respect to z. The diffusion coefficients are listed in appendix A.

Since the left- and right-handed quarks have approximately equal diffusion constants, baryon number is locally conserved on the time scale of the transport equations such that

$$t + b + q + c + s + q_2 + u + d + q_1 = t + b + q = 0\,. \tag{5.37}$$

In the second expression we used that the light quarks are only produced via strong sphalerons eq. (5.31). Local baryon number conservation can be used to eliminate the transport equation for the bottom quark. The set of transport equations can be further simplified by neglecting the slower rates, but which rates can be neglected depends on the chosen source term. If bottom Yukawa interactions are neglected we have $b = u$, and the number densities of all quarks directly follow from (q, t). If bottom Yukawa interactions are included we additionally have to solve the u-equation.

In contrast, lepton number is only conserved globally [273]. Right-handed leptons diffuse more easily than left-handed leptons since right-handed leptons do not interact through $SU_L(2)$-interactions, and therefore $D_l \neq D_\tau$. As we will see in chapter 7, for our set-up it is a reasonably good approximation to neglect this difference and assume local lepton number conservation as well.

5.5 Electroweak sphalerons

The electroweak sphalerons convert the chiral asymmetry into a baryon asymmetry. The corresponding rate is slower than all other relevant interaction rates and thus decouples from the transport equations. The only exception is the lepton Yukawa rate and we discuss this case in section 7.3. The density of left-handed fermions that sources the electroweak sphaleron transitions is given by $n_L = \sum_i (q_i + l_i)$, and is determined by solving the transport equations (5.32). The baryon asymmetry becomes (see Appendix B of Ref. [4] for a derivation)

$$Y_B = \frac{n_b}{s} = -\frac{3\Gamma_{\rm ws}}{2sD_q\alpha_+}\int_{-\infty}^{0} \mathrm{d}z\, n_L \mathrm{e}^{-\alpha_- z}\,, \qquad \alpha_\pm = \frac{v_w \pm \sqrt{4D_q\Gamma_{\rm ws}\mathcal{R} + v_w^2}}{2D_q}\,. \tag{5.38}$$

Here $s = 2\pi^2/(45) g_{*S} T^3$ is the entropy density, $g_{*S} = 106.75$ the entropy degrees of freedom at the electroweak scale, $D_q \simeq 6/T$ the quark diffusion constant, $\mathcal{R} = 15/4$ the SM relaxation term, and $\Gamma_{\rm ws} = 6\kappa\alpha_w^5 T$ the electroweak sphaleron rate with $\kappa \sim 20$ and $\alpha_w = g^2/(4\pi)$ [274–276]. In the limit $4D_q\Gamma_{\rm ws}\mathcal{R} \ll v_w^2$, the result reduces to a more familiar form

$$Y_B = \frac{n_b}{s} = -\frac{3\Gamma_{\rm ws}}{2v_w s}\int_{-\infty}^{0} n_L(z)\, e^{z\,\mathcal{R}\Gamma_{\rm ws}/v_w}\,. \tag{5.39}$$

This approximation works well for $v_w \geq 0.02$. We integrate the asymmetry over the broken phase ranging from $z = -\infty$ to the center of the bubble wall at $z = 0$ where $\varphi_b = v_N/2$. Other integration regions can be chosen, for instance $-\infty < z < -L_w$ [252, 273]. This gives a percent-level difference for the asymmetry generated by a lepton source, but can give an $\mathcal{O}(1)$ difference for the top source.

It would be optimal to integrate over the full region using the field-dependent $\Gamma_{\rm ws}(\varphi_b)$, but this requires a better understanding of the electroweak sphaleron rate.